NREL/TP-411-5063 • UC Category: 271 • DE93000011

Research on Stable, High-Efficiency Amorphous Silicon Multijunction Modules

Semiannual Subcontract Report 1 January 1992 – 30 June 1992

NREL/TP--411-5063

DE93 000011

S. Guha
United Solar Systems Corporation
Troy, Michigan

NREL technical monitor: W. Luft

National Renewable Energy Laboratory
1617 Cole Boulevard
Golden, Colorado 80401-3393
A Division of Midwest Research Institute
Operated for the U.S. Department of Energy
under Contract No. DE-AC02-83CH10093

Prepared under Subcontract No. ZM-1-19033-2

September 1992

On September 16, 1991 the Solar Energy Institute was designated a national laboratory, and its name was changed to the National Renewable Energy Laboratory.

Printed in the United States of America
Available from:
National Technical Information Service
U.S. Department of Commerce
5285 Port Royal Road
Springfield, VA 22161

Price: Microfiche A01
Printed Copy A03

Codes are used for pricing all publications. The code is determined by the number of pages in the publication. Information pertaining to the pricing codes can be found in the current issue of the following publications which are generally available in most libraries: *Energy Research Abstracts (ERA)*; *Government Reports Announcements* and Index (*GRA* and I); *Scientific and Technical Abstract Reports (STAR)*; and publication NTIS-PR-360 available from NTIS at the above address.

Preface

This Semiannual Subcontract Report covers the work performed by United Solar Systems Corp. for the period 1 January 1992 to 30 June 1992 under DOE/NREL Subcontract Number ZM-1-19033-2. The following personnel participated in the research program.

> A. Banerjee, E. Chen, T. Glatfelter, S. Guha (Principal Investigator), G. Hammond, M. Hopson, N. Jackett, M. Lycette, T. Palmer, I. Rosenstein, D. Wolf, J. Yang, X. Xu and K. Younan.

The small-angle X-ray scattering experiments reported in Section 2 were carried out at the Colorado School of Mines by D. L. Williamson, S. J. Jones and Y. Chen, and we thank them for this collaborative effort.
0
We would like to thank V. Trudeau for preparation of this report.

Table of Contents

List of Figures

List of Tables

Executive Summary

Objectives

The principal objective of the program is to conduct research on semiconductor materials and non-semiconductor materials to enhance the performance of multi-bandgap, multijunction, large-area amorphous silicon-based alloy modules. The goal for 1992 is to demonstrate stabilized module efficiency of 10% for multijunction panel of area greater than 900 cm^2.

Approach

Double-junction and triple-junction cells are made on Ag/ZnO back reflector deposited on stainless steel substrates. a-SiGe alloy is used for the *i*-layer in the bottom and the middle cells; the top cell uses a-Si alloy. After evaporation of antireflection coating, silver grids and bus bars are put on the top surface, and the panel is encapsulated in an ethylene vinyl acetate (EVA)/Tefzel structure to make a one-square-foot monolithic module.

Status/Accomplishments

- Using a combination of small-angle scattering and infrared absorption measurements on a-Si alloy films and efficiency measurements on cells, we find that there is a correlation between the microstructure of the films and cell performance. Both the initial and the stabilized performance of solar cells deteriorate when the microvoid density in the films becomes larger.

- The annealing kinetics of the metastable defects is also found to depend on the density of microvoids in the films. With increasing microvoid density, some light-induced defects are created which are harder to anneal out.

- A detailed investigation of film property and cell performance using a-SiGe alloys with different germanium contents shows that there is no good correlation between defect density measured by constant photocurrent method and cell performance.

- We have studied the stability of various dual-bandgap, double-junction cells in terms of the bandgaps of the bottom cells and the current mismatch between the component cells. Using a bandgap-profiled bottom cell and optimized current mismatch, we have achieved active-area (0.25 cm^2) efficiency of 11.16% as measured using a single-source simulator after 600 h one-sun 50°C illumination. **This is the highest stabilized small-area efficiency reported for a-Si alloy solar cells.** A similarly degraded cell measured under NREL dual-source simulator showed an active-area efficiency of 10.4%.

- We have made a large number of double- and triple-junction modules with aperture area larger than 900 cm^2 showing initial efficiencies exceeding 9%. The highest initial aperture area efficiency measured indoors at NREL on our modules is 9.3%. **This is the highest initial aperture area efficiency measured by NREL on multi-bandgap, multijunction** panels with area larger than 900 cm^2. The same module measured 9.6% under the USSC Spire simulator. Our light-soaking measurements indicate typically 15% degradation in these panels after 600 h one-sun exposure at 50°C.

Section 1

Introduction

The research program is directed toward advancing our understanding of amorphous silicon alloys and other relevant non-semiconductor materials for use in large-area multijunction modules. An important thrust of the program is on performance of modules after long-time light exposure; therefore, study of light-induced degradation forms an important part of the program. The goal of this phase of the program is to demonstrate a stable, aperture-area efficiency of 10% for a two-terminal, multi-bandgap, multijunction module of aperture area of at least 900 cm^2 by 1992.

The program is divided into three tasks. Task I, semiconductor materials research, is directed toward depositing, optimizing and characterizing of suitable amorphous silicon alloy materials and cell structures over 900 cm^2. Task 2, non-semiconductor materials research, involves investigating suitable back reflectors and antireflection coatings and also encapsulants for the modules. Task 3, module research, is directed toward fabricating modules involving grid patterning, cell isolation and interconnect, and encapsulation.

In this report, we outline the progress made toward the program goal in the different task areas. In Section 2, we discuss the results of fundamental studies on materials and cells in which the intrinsic layers are deposited at different rates. We demonstrate that microstructure of the material has profound influence on cell efficiency and stability. We also discuss an optimized cell design using a double-junction structure which gives a stable active-area (0.25 cm^2) efficiency of 11.2%. In Section 3, we discuss our large-area deposition status and report active-area (0.25 cm^2) initial efficiencies of 11.4% for double-junction and 11.15% for triple-junction structures. The corresponding efficiencies obtained from our small-area deposition reactor range from 12.5% to 13%. The possible causes for the difference in efficiencies between the small-area and large-area deposition reactors are discussed. In Section 4, we discuss the status of the module research. A large number of modules has been fabricated with initial aperture efficiencies exceeding 9%. The highest efficiency achieved is 9.6% which when measured at NREL shows 9.3%. Typical degradation for the modules after light-exposure is about 15%.

Section 2

Materials and Cell Research

Introduction

In order to obtain a basic understanding of the origin of as-grown and light-induced defects in a-Si alloy films and cells, we have carried out investigations on both material properties and cell performance using materials deposited under similar conditions. The first investigation addressed the issue of correlation between microstructure of the material and cell performance where the microstructure was altered by changing the deposition rate of the intrinsic layer. Both the defect generation and annealing were investigated. We also measured the defect density in amorphous silicon-germanium alloys with different germanium content and the corresponding cell performance. The aim was to determine if film measurements are adequate to predict cell performance. Finally, we investigated the effect of mismatch of the component cells in a double-junction structure to arrive at an optimum design for obtaining the highest stabilized efficiency.

Microvoids and Cell Performance

Light-induced degradation of hydrogenated amorphous silicon (a-Si:H) alloy materials and devices has been the subject of intensive studies.[1] It is generally agreed that recombination of excess electron-hole pairs generated by illumination creates metastable defects in the bulk of the material.[2] The defect states reduce the mobility-lifetime product of electrons and holes and causes degradation of solar cell performance. The origin of the metastability is not quite understood, and the list of causes includes[3] hydrogen, impurities like C, O or N, microvoids due to inhomogeneous growth, weak bonds or a combination of these.

Using small-angle X-ray scattering (SAXS) measurement, it has been recently demonstrated[4,5] that even in the best quality material, microvoids of typical diameter 1.0 nm exist, occupying a volume fraction of about 1%. The void density is typically larger for poorer quality material.[6] In order to correlate the microvoid density in the material with the initial and light-degraded performance of solar cells, we have fabricated single-junction *p i n* solar cells in which the intrinsic layer has different microvoid density caused by changes in the deposition rate. The results are reported in this report.

Single-junction *p i n* solar cells were grown by the rf glow-discharge technique on stainless steel substrates kept at 300°C. Details of deposition parameters are given elsewhere.[7] The intrinsic layer was grown using a disilane-hydrogen mixture, and the dilution of the mixture and rf power density were changed to obtain deposition rates between 0.14 and 1.35 nm/sec. The thicknesses of the *i*-layers were kept constant at ~ 420 nm. The deposition conditions for the doped layers were kept the same for all the samples. The top contact was made using thermally evaporated indium tin oxide (ITO). Cell performance was measured under global AM1.5, red, and blue illumination.

Samples consisting of only the *i*-layer, typically 1 μm thick, were deposited separately on crystalline silicon wafers for infrared (IR) measurements and on thin, iron-free, high-purity Al foils for SAXS measurements. The deposition conditions were nominally identical to those used to produce solar cells. Details of the SAXS experimental methods have been discussed elsewhere.[8]

Figure 1 shows the SAXS data for three samples prepared with different deposition rates where the natural log of the normalized scattering intensity[8] is plotted versus the magnitude of the scattering vector h and compared to the SAXS signal from a 70 μm crystalline Si wafer (polished on both sides). There is a clear systematic increase in the SAXS signal with increasing deposition rate. Above about 2 nm^{-1} the SAXS intensity is essentially angle independent for the 0.14 and 0.62 nm/sec deposition rates, and we believe this is due primarily to Laue monotonic scattering[9] by the Si-H alloy matrix which should increase with increasing H content. This accounts for most of the difference between the crystalline Si and the two lower deposition rate a-Si:H films above h=2 nm^{-1}. The film grown with the highest rate clearly shows angular dependence in the SAXS up to the largest angles. After correcting for the angle-independent contribution for all three samples, we estimate the volume fraction of voids (V_f) assuming a simple two-phase system (voids and matrix) as described in detail elsewhere.[6,8] We find similar values of V_f of 1 ± 0.5% for the samples prepared with 0.14 and 0.62 nm/sec deposition rates and 4 ± 1% for the one deposited with the 1.35 nm/sec rate.

In order to explore the shape and orientation characteristics of the voids, the sample with the largest void-fraction was measured at a tilt angle of 45°, and the results are compared to the non-tilted data in Fig. 2. The data are identical within experimental error, and this demonstrates that the voids are of spherical shape or, if non-spherical, randomly oriented throughout the sample.[6]

The sample with the large void fraction was also analyzed to extract the approximate void size distribution by fitting a superposition of SAXS curves due to a few distinct spherical microvoid diameters and adjusting the sizes and volume fractions to give a good fit. We estimate that about 80% of the void volume is due to diameters of 0.9 nm with most of the remainder less than 10 nm in diameter. The very small voids account for most of the increase in V_f compared to the two films prepared at the lower deposition rates.

The initial and light-degraded (after 600 h one-sun, 50°C, open-circuit condition illumination) performances of the solar cells as a function of *i*-layer deposition rate are shown in Fig. 3. The initial efficiency is found to decrease above deposition rates of ~ 0.35 nm/sec. The light-degraded efficiency shows a systematic, continuous decrease as the deposition rate is increased. It is interesting to note that at a deposition rate of 0.14 nm/sec, the relative degradation is only 12.5% whereas at 1.35 nm/sec, the relative degradation is 43%. We should mention that since the samples are deposited on stainless steel, both the initial and final efficiencies are lower than those on an optimized back reflector. A reference cell of the same thickness deposited on Ag/ZnO back reflector at a deposition rate of 0.14 nm/sec has an initial efficiency of 11% and degrades by about 30% under the same light-soaking condition. Since photon absorption is enhanced with a back reflector, the generation rate of carriers is larger, and this results in a higher degradation.

Since increasing deposition rate leads to higher void density, the results indicate an enhancement in degradation of solar cells with the *i*-layers having more microstructure. This is consistent with earlier results[10] which showed an increase in light-induced sub-bandgap absorption in films that showed more microstructure as determined by the ratio of infrared absorption at wave numbers 2070 cm^{-1} and 2000 cm^{-1}. For our films deposited at 0.14 nm/sec, the hydrogen content is 8% whereas that for the deposition rate of 1.35 nm/sec is 12%. The ratio of the microstructure fraction, R, as defined by $R = I_H(2070)/[I_H(2000) + I_H(2070)]$ increases from 8.4% to 18.4% in these two films. $I_H(2000)$ and $I_H(2070)$ are the integrated infrared absorption due to the stretching mode bonds at 2000 cm^{-1} and 2070 cm^{-1}, respectively.[11] It should be pointed out that although R increases from 8.4% to 18.4% as the deposition rate is raised from 0.14 nm/sec to 1.35 nm/sec, C_H (2000), which is the concentration of hydrogen bonded in the Si-H monohydride mode at 2000 cm^{-1}, remains constant at around 6.4%. This suggests that, at least in these films, the degradation process is not associated with the isolated Si-H bonds in the dense amorphous

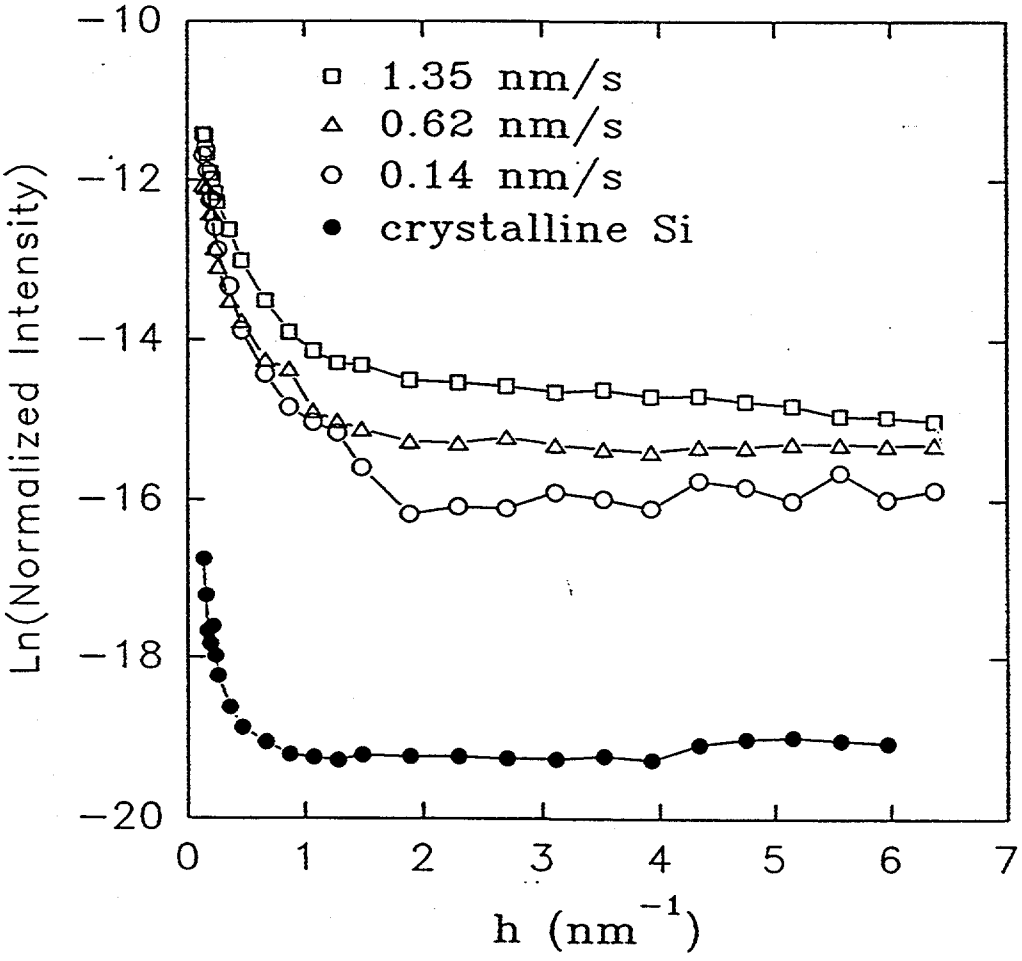

Fig. 1. SAXS data for a-Si alloy films grown at different deposition rates compared to data from a crystalline Si wafer. The intensity has been normalized and corrected for substrate effects according to the procedure in ref. 8. $h=4\pi\sin\theta/\lambda$, where $\lambda=0.154$ nm and 2θ is the scattering angle. The solid lines are drawn to connect the data points.

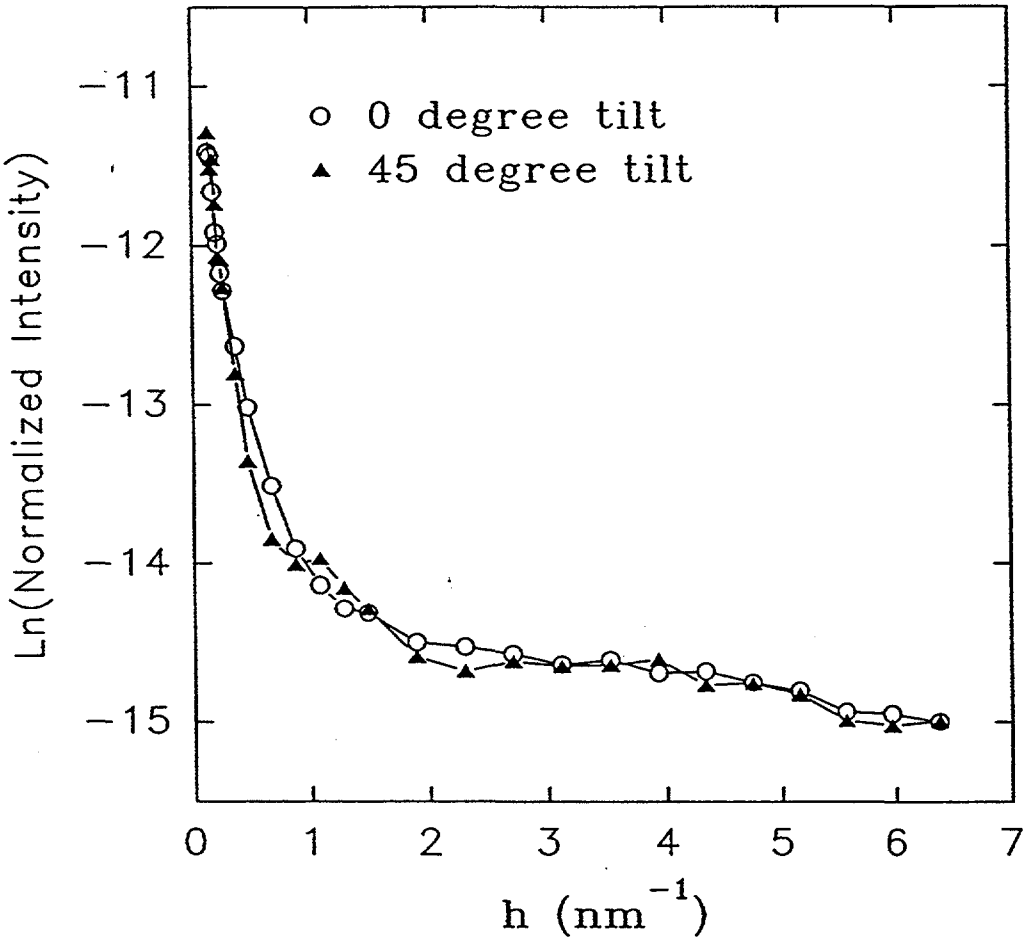

Fig. 2. SAXS data from the sample grown at 1.35 nm/sec mounted in two orientations relative to the X-ray beam

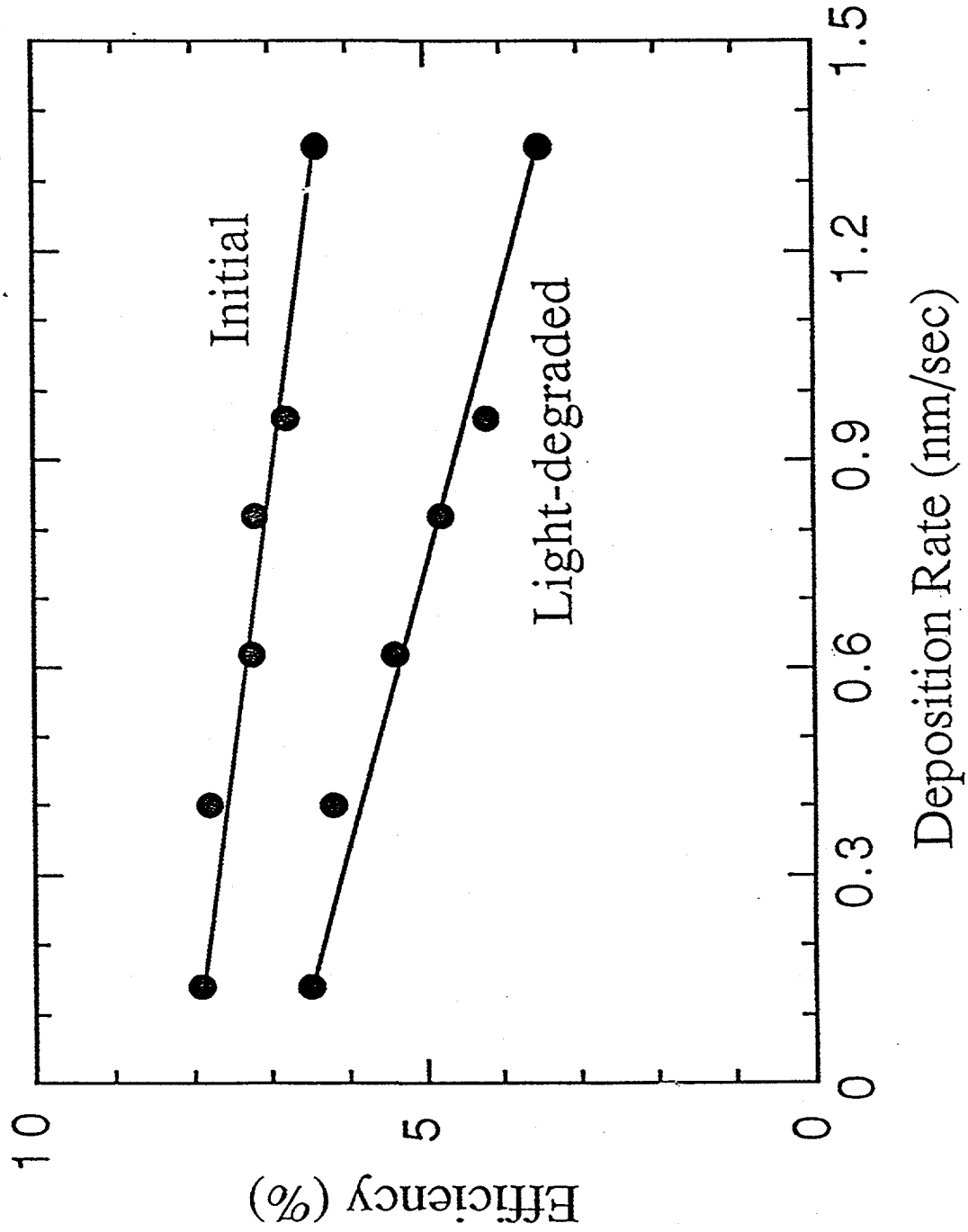

Fig. 3. Initial and light-degraded efficiencies of a-Si alloy solar cells as a function of deposition rate

matrix. It also suggests that the increased angle-independent SAXS contribution with increasing deposition rate (proposed above to be the Laue monotonic scattering from increased H in the a-Si:H matrix) is not due to increased numbers of isolated Si-H bonds but rather to bonds associated with the 2070 cm^{-1} mode.

Our results, showing increased light-degradation in materials with larger void-fraction and microstructure fraction, do not support the suggestion by Matsuda et al.[12] that material with increased microstructure may be more stable. Their conclusion was based on photoconductivity measurements on materials deposited from Xe-diluted silane mixtures. The dangling bond density, both in the initial and light-degraded state, was, however, found to be higher for films with poorer microstructure. As we shall discuss below, this is in agreement with our solar cell results.

We should mention that our results show a decrease both in the initial and degraded performance of the solar cells with increase in the density of microvoids whereas the results of Bhattacharya and Mahan[10] showed no change in the initial quality of the film as determined by sub-bandgap absorption even when R was as high as 50%. The sensitivity in measurement of solar cell efficiency, of course, is much better than that in defect density estimation from sub-bandgap absorption. The deterioration of the material quality as a function of increased microstructure is evident from Table I where we have tabulated results from both microstructure and solar cell measurements for samples prepared at a deposition rate of 0.14 nm/sec and 1.35 nm/sec. The fill factor under red and blue illumination is determined by the collection length of the photo-generated carriers which, in turn, is governed by the defect density. A clear correlation between both initial and light-degraded defect density and void density is apparent. Since dangling bonds are the predominant defect centers in a-Si:H films, these results are in agreement with those reported in Ref. 12. We would like to point out that although we see a correlation between deposition rate and void density, these results should be considered only to depict the trend under certain deposition parameters. With different gas mixtures or at a different substrate temperature, it may be possible to get a lower void density even at a higher deposition rate.

In conclusion, by a combination of IR and SAXS measurements on films and efficiency measurements of solar cells, we see a correlation between microstructure and solar cell performance. With increasing microvoid density and microstructure fraction, both the initial and light-degraded solar cell performance are found to deteriorate.

Table 1. Material Properties and Cell Performance for Samples Prepared at Two Different Deposition Rates

Deposition rate	0.14 nm/sec	1.35 nm/sec
Void fraction	1%	4%
Predominant void diameter	-	0.9 nm
Hydrogen content	8%	12%
Microstructure fraction (R)	8.4%	18.4%
C_H (2000)	6.4%	6.3%
Initial efficiency	7.85%	6.31%
Degraded efficiency	6.53%	3.5%
Initial red fill factor	0.67	0.52
Degraded red fill factor	0.52	0.43
Initial blue fill factor	0.73	0.67
Degraded blue fill factor	0.67	0.40

Annealing Behavior of the Metastable Defects

Since microstructure plays an important role in determining both the as-grown and the metastable defect densities, it is interesting to find out if it influences the annealing behavior of the defects as well. Table 2 shows the recovery of the cells reported in Sec. 2.2 after annealing at 150°C for 90 minutes. η_I is the initial efficiency, η_D is the efficiency after one-sun light soaking for 600 h at 50°C and η_A is the efficiency after subsequent annealing at 150°C for 90 minutes. It is interesting to note that as the deposition rate increases, the recovery is slower as if there are some defects which are harder to anneal. After prolonged heating at 190°C for 10 hours, the cell efficiencies could be restored to their initial values.

There have been several reports describing different annealing behaviors of metastable defects in materials prepared or illuminated under different conditions. It has been reported that metastable defects in B-doped a-Si alloys are easier to anneal.[13] Addition of impurities like O, N or C in quantities in excess of 1% also affect the annealing kinetics of the metastable defects.[14] Even in undoped material, the annealing behavior of the defects is governed by the conditions under which the defects are created. Defects created under light exposures at higher temperature[15] or for longer time[16] are known to be more difficult to anneal out. This is, however, the first evidence that defect annealing is related to microstructure of the material. If annealing of the metastable defects is related to hydrogen transport, one would expect the hydrogen diffusion constant to be smaller for the structure with more microvoids. It is possible that the microvoids act as trapping sites for the hydrogen thus slowing down its motion. Another way of explaining the dependence of annealing behavior on microvoids is by assuming larger energy barriers between the stable and the metastable configurations with increasing microstructure. Further experiments will be necessary to understand this annealing behavior.

Table 2. Annealing Behavior of Light-degraded Efficiency for Cells with Different *i*-layer Deposition Rates

Deposition Rate (Å/s)	1.4	3.5	6.2	13.5
η_I	7.78%	7.80%	7.29%	6.31%
η_D	6.81%	6.47%	5.49%	3.58%
η_D/η_I	87.5%	82.9%	75.3%	56.7%
η_A	7.42%	7.20%	6.18%	4.93%
η_A/η_I	95.4%	92.3%	84.8%	78.1%

Correlation Between Film Property and Cell Performance

It is generally agreed that the degradation in efficiency of solar cells is predominantly caused by deterioration of the material quality. A great deal of effort, therefore, has been made to investigate material property before and after light-induced degradation to obtain the best material for optimized solar cell performance.

The most commonly used techniques to evaluate material properties are the measurement of photoconductivity and sub-bandgap absorption. Using uniformly absorbing monochromatic light to measure the photocurrent, one can obtain the majority carrier $\mu\tau$ product in the material. Measurement of sub-bandgap absorption by photothermal deflection spectroscopy (PDS) or by constant photocurrent method (CPM) gives information about the valence band tail and the near mid-gap deep states. Integration of the sub-bandgap absorption can be correlated to the spin density in the material[17] and has been used to predict solar cell performance.[18]

The applicability of the use of defect density obtained from CPM to predict the solar cell performance, however, merits careful scrutiny. It is widely recognized[19] that the accuracy of the defect density obtained from sub-bandgap absorption measurement depends critically on several factors such as the precision of matching the sub-bandgap CPM or PDS data to absorption values measured at higher than bandgap energy and also on the accuracy of determining the slope of Urbach edge. An uncertainty of a factor of 2 to 3 in the estimated value is easily expected. A change in the defect density by a factor of 2, however, will drastically affect the solar cell performance.

In order to determine the degree of correlation that exists between material properties and solar cell performance, we have studied the material properties of a-SiGe alloy films and also the performance of cells with the intrinsic layers deposited under nominally identical conditions. The results are reported in this paper.

a-SiGe alloy films, typically 1 μm thick, were deposited on crystalline silicon wafer and 7059 glass substrates from a dilute mixture of disilane and germane.[20] The germane flow was varied to obtain films with three different bandgaps. Single-junction *n i p* solar cells were made on stainless steel with predeposited textured Ag/ZnO back reflector. The intrinsic layers of the cells, typically 3000 Å thick, were grown under conditions nominally identical to those for the films deposited on glass.

The films on glass substrates were characterized by measurement of dark and photoconductivity, above-bandgap optical absorption and reflection and sub-bandgap absorption by photothermal deflection spectroscopy and constant photocurrent method. Infrared absorption measurement was used to determine the hydrogen content of the films deposited on silicon wafers. The solar cell performance was measured under global AM1.5 illumination and also under red and blue illumination. In Table 3, we show the properties of three films with different germanium contents. The mobility-lifetime ($\mu\tau$) product for electrons is measured with 750 nm light of an incident flux of 5.10^{14} cm^{-2} sec^{-1}. The Urbach edge (E_u) was obtained from PDS measurement, and the defect density is calculated from integrated sub-bandgap absorption below the Urbach edge as measured by CPM. We notice that the Urbach edge remains constant with increasing Ge-content; the $\mu\tau$ product, however, decreases with increasing Ge-content. The defect density for the three samples is in the range from 3 to 5.6 x $10^{15}/cm^3$. Also shown in Table 3 are the properties after one-sun light-soaking at 50°C for 600 h. The $\mu\tau$-products decrease for all the three samples as a result of the light-soaking. The defect density increases by about a factor of 2 for the films with lesser Ge-content. For the film with 41% Ge, however, the defect density remains unchanged from the as-deposited condition.

Table 3. Properties of a-SiGe Alloys with Different Ge-content

Sample	Ge-Content (%)	Optical Gap (eV)	Eu (meV)	μτ ($cm^2V^{-1}S^{-1}$)		Defect Density (cm^{-3})	
				Init.	Degraded	Init.	Degraded
4827	19	1.55	51	$8x10^{-7}$	$2.7x10^{-7}$	$5.1x10^{15}$	$1.2x10^{16}$
4830	30	1.50	52	$3x10^{-7}$	$1.5x10^{-7}$	$3.1x10^{15}$	$6.6x10^{15}$
4829	41	1.41	49	$1x10^{-7}$	$4.0x10^{-8}$	$5.6x10^{15}$	$6.5x10^{15}$

In Fig. 4 we show the initial and light-degraded efficiencies of cells where the *i*-layers are about 3000 Å thick and have been grown under nominally identical conditions to those for the films shown in Table 3. All the cells show typical light-induced degradation between 30 to 40%. In Table 4, we tabulate the performance of the cells under global AM1.5, blue and red illumination. We notice that the maximum degradation is in the fill factor of the cells. For the cell with the largest bandgap, the blue fill factor remains unchanged, whereas the red fill factor degrades by a small amount. For the cells with lower bandgap, both the red and the blue fill factors show larger degradation. The fill factor of a solar cell is essentially governed by the ease with which the photogenerated carriers can be collected at the electrodes. For the highly absorbing blue photons, the fill factor is determined by the electron transport, whereas for the more uniformly absorbing red photons, the carrier with the poorer transport property will determine the fill factor. For example,[21] in high quality a-Si alloy single-junction cells, the blue fill factor is much better than the red fill factor because the μτ product for electrons is much higher than that for the holes. It is interesting to note that for all the three a-SiGe alloy cells shown in Table 4, the red and the blue fill factors are very similar in the undegraded state even though the μτ product for electrons drops down drastically with increasing Ge-content. What is more interesting is the fact that even though the defect density as measured by CPM hardly changes after light-soaking in the lowest bandgap alloy, the corresponding cell shows a large degradation in both the red and the blue fill factors. We should also point out the lack of correlation between the μτ value and the defect density in the a-SiGe alloys. This is partly due to the fact that even if the defect density remains the same, with increasing Ge-content, the electron mobility decreases, which would cause the μτ product to be lower.[22] It is interesting, however, that for the lowest bandgap alloy, even though the μτ product degrades after light-soaking, the defect density does not change much. The dark conductivity of the sample is about the same in the degraded and the annealed states, and a shift in the Fermi level cannot explain this anomaly. As we have pointed out earlier, there can easily be an error by a factor of 2 in the estimate of defect density of different samples. On the same sample, however, the accuracy is much better. There must be, therefore, other changes taking place after light-soaking which affect the solar cell performance, but cannot be detected by CPM. New states may be created above the Fermi level; the capture cross-section of the light-induced states also could be different. CPM would be insensitive to these changes.

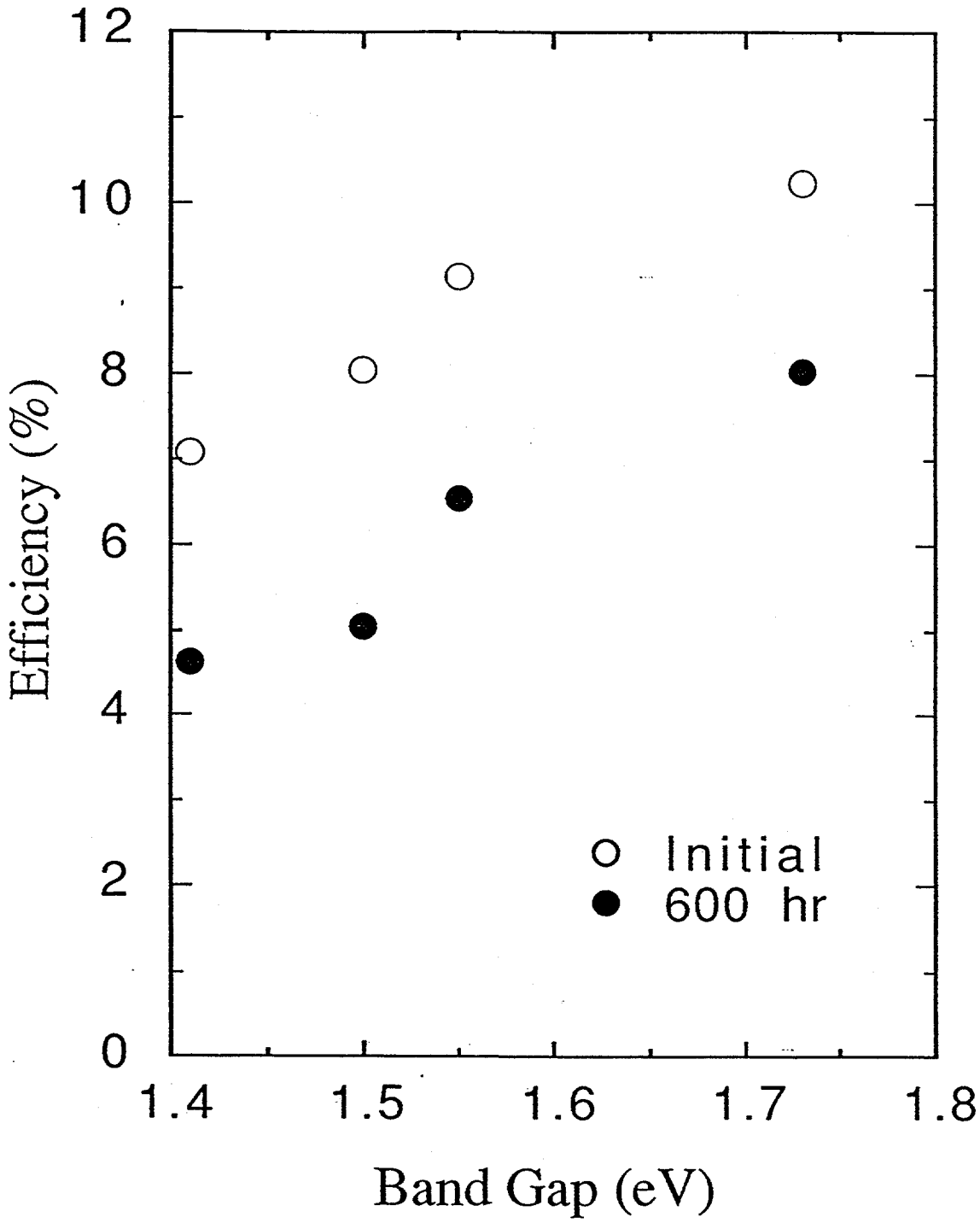

Fig. 4. Initial and light-degraded efficiencies of single-junction solar cells as a function of bandgap of the intrinsic layer

Table 4. Performance of Single-junction a-SiGe Alloy Solar Cells before and after Light Soaking for 600 Hours under One-sun Illumination at 50°C

i-layer Bandgap	State	AM1.5 Performance J_{sc} (mA/cm^2)	V_{oc} (V)	FF	η (%)	Fill Factor Blue	Red
1.55 eV	Initial	18.50	0.80	0.62	9.18	0.60	0.59
	Degraded	17.21	0.76	0.50	6.54	0.59	0.54
1.50 eV	Initial	20.93	0.70	0.55	8.06	0.58	0.60
	Degraded	17.81	0.66	0.43	5.05	0.48	0.46
1.41 eV	Initial	22.39	0.61	0.52	7.10	0.60	0.59
	Degraded	19.92	0.57	0.40	4.54	0.49	0.48

We would like to emphasize that the observed lack of correlation does not imply that measurement of film property cannot give general ideas about the solar cell performance. If the $\mu\tau$ product is very low or the defect density very high, the solar cell will also perform poorly. However, with the current accuracy of CPM measurements, it is not possible to distinguish between high-quality materials where the defect densities differ by a factor of 2 or less. Moreover, as discussed earlier, factors other than the density of deep states also affect solar cell performance.

In conclusion, we have studied the performance of a-SiGe alloy single-junction solar cells both before and after light-soaking. The intrinsic layers of the cells have different Ge-contents. a-SiGe alloy films were grown on glass with parameters nominally identical to those for the cells, and the film properties were measured. We do not find good correlation between cell performance and film properties for these high-quality materials.

Stability Study on Double-junction Cells

We have previously reported[23] that initial conversion efficiencies of ≥ 13% can be achieved in amorphous silicon-based multijunction solar cells. In this letter, we report the results of our stability study on various dual-bandgap, double-junction devices in which the top and bottom cells were made from hydrogenated amorphous silicon (a-Si:H) and hydrogenated amorphous silicon-germanium (a-SiGe:H) alloys, respectively.

To obtain a high-performance, double-junction cell, the component cells should have high efficiency and stability. However, the quality of the narrow bandgap a-SiGe:H material is usually poorer than that of a-Si:H. One can get better results by mismatching the cells so that the limiting cell is the a-Si:H cell, which has a better fill factor.

We have fabricated various double-junction 0.25 cm^2 devices in which the bottom a-SiGe:H cells have bandgaps ranging from 1.41 to 1.55 eV. We have studied the effect of bandgap variation and current-mismatching on the stability of the double-junction devices. Most of the devices investigated stabilized at an active-area efficiency of about 10% while the best performance was obtained from incorporating a profiled bandgap in the bottom cell having a bandgap of 1.41 eV at the narrowest region. A stabilized active-area efficiency of 11.16% was observed after 600 hours of one-sun illumination at 50°C. This is believed to be the highest stabilized value reported to date on amorphous silicon-based double-junction solar cells.

To study the effect of bandgap variation, we made three double-junction samples in which the bottom cells have a constant bandgap of 1.55 eV (L4781), 1.50 eV (L4786), and 1.41 eV (L4801), respectively, and the top cells were made from 1.75 eV a-Si:H material using the same deposition parameters. These samples were deposited onto stainless steel/textured silver/zinc oxide substrates using the conventional RF glow discharge technique. The thickness of the top cells was made small so that the fill factor is high and the current of the double-junction device is limited by the top cell. This would allow us to evaluate the effect of the bottom cell on the stability of the double-junction structure. The initial performance of these devices measured under a global AM1.5 solar simulator is listed in Table 5. It is noted from the quantum efficiency data that the current is limited by the top cell, and the mismatch between the top and bottom cells ranges from 1.5 to 3 mA/cm^2.

We have also made a double-junction device (L4808) in which the thickness of the top cell was made larger such that the top cell current is nearly the same as that of the bottom cell. In this case, we have used the 1.55 eV a-SiGe:H cell in the bottom cell. The initial performance of the double-junction device is also listed in Table 5. The quantum efficiency data confirms that the two currents are nearly matched.

These samples were then light-soaked with one-sun illumination at 50°C under open-circuit condition for 600 hours. Their degraded J-V characteristics and quantum efficiency data are also listed in Table 5.

Table 5. Initial and Stabilized Photovoltaic Characteristics of Various Dual-gap, Double-junction Devices

Sample	State	J_{sc} (mA/cm^2)	V_{oc} (V)	FF	η (%)	Q (mA/cm^2)
L4801	Initial	9.60	1.60	0.73	11.21	9.35/12.27
(1.41 eV)	600 hrs	9.52	1.55	0.68	9.97	9.21/11.71
L4786	Initial	9.70	1.65	0.74	11.84	9.47/11.42
(1.50 eV)	600 hrs	9.70	1.59	0.67	10.36	9.46/10.86
L4781	Initial	9.67	1.68	0.74	12.02	9.43/10.89
(1.55 eV)	600 hrs	9.66	1.61	0.66	10.24	9.29/10.65
L4808	Initial	10.05	1.66	0.70	11.68	10.24/10.49
(1.55 eV)	600 hrs	9.98	1.60	0.62	9.88	10.07/10.38

Each sample consists of several 0.25 cm^2 active-area devices. The measurements were made using a single-source AM1.5 solar simulator at 25°C. The Q-values refer to the top cell and the bottom cell, respectively.

One can readily make the following observations:

1. On the initial performance of L4781, L4786, and L4801:

   a. As the bandgap of the bottom cell decreases, V_{oc} also decreases as expected. Sample L4801, which has the narrowest bandgap in the bottom cell, exhibits the largest current mismatch between the component cells.

   b. J_{sc} and fill factor are similar for the three devices because of the same deposition parameters used for the current-limiting top cells.

   c. The initial efficiency of the double-junction devices is hence essentially dependent on V_{oc}. Sample L4781, which has the least Ge in the bottom cell, shows the highest initial efficiency.

2. The initial performance of sample L4808, which has the same bottom cell as L4781, exhibits a higher J_{sc} value because of the thicker top cell. However, the fill factor of the devices is lower than the other three samples due to the closer match. Its V_{oc} is also slightly smaller than L4781 due to the thicker top cell.

3. On the degraded J-V characteristics of samples L4781, L4786, and L4801:

   a. Sample L4801, which has the narrowest bandgap in the bottom cell, shows the lowest V_{oc}, consistent with the initial performance.

   b. Sample L4801 has a slightly better fill factor due to the larger current mismatch.

   c. J_{sc} remains similar for the three samples.

   d. The percentage of degradation and stabilized efficiencies are similar for the three samples.

4. The degraded performance of sample L4808, which has a thicker top cell than L4781, shows a lower fill factor due to closer matched component cells, and J_{sc} remains higher due to the thicker top cell.

From the above analysis, one can see that in order to achieve a higher stabilized efficiency, one should current-limit the top cell. The desired amount of mismatch depends on the performance of the bottom cell. If the performance of the bottom cell is improved, the mismatch can be reduced, and one can then take advantage of a thicker top cell for higher J_{sc} without losing too much on the fill factor.

We have designed a double-junction device in which we have incorporated a profiled bandgap structure in the bottom a-SiGe:H cell which we have previously shown to improve solar cell performance.[24] The bandgap in the narrowest region is 1.41 eV, and the top cell is 1.75 eV a-Si:H. The initial performance of this device is listed in Table 6. After 600 hours of one-sun illumination at 50°C, the stabilized active-area efficiency as measured under global AM1.5 single-source simulator at 25°C is 11.16%, which we believe is the highest value reported to date on double-junction amorphous silicon alloy solar cells. A similarly degraded cell, measured at NREL under a dual-source simulator, showed an active-area efficiency of 10.4%.

Table 6. Initial and Stabilized Photovoltaic Characteristics of a Dual-gap, Double-junction 0.25 cm² Device with Profiled Bandgap in the Bottom Cell

Sample	State	J_{sc} (mA/cm²)	V_{oc} (V)	FF	Active Area (cm²)	η (%)
L4789	Initial	10.67	1.650	0.716	0.2465	12.61
	600 hrs	10.61	1.606	0.655	0.2465	11.16

In summary, we have studied the stability of various double-junction solar cells in terms of the bandgaps of the bottom cells and current mismatch between component cells. We have used a bandgap profiling structure as well as a current mismatch approach and obtained a high stabilized conversion efficiency of 11.16%.

Section 3

Large-area Deposition Research

Introduction

The 2B machine has been used to prepare cells for large-area (~ 900 cm^2) module fabrication. Two types of cell structures have been investigated: dual-bandgap, double-junction cells and triple-bandgap, triple-junction cells. The top cell in both structures consists of an a-Si:H *i*-layer, and the middle and bottom cells have a-SiGe:H alloy *i*-layers. The back reflector in all cases is ZnO/Ag/stainless steel.

The cell fabrication procedure consists of first preparing the back reflector using sputter deposition technique. The coated area is greater than 900 cm^2. The substrate with the back reflector is then inserted in the 2B machine for the deposition of the *n*-, *i*- and *p*-layers. Next, the substrate is either cut into smaller pieces for (1) small-area research or processed as such for (2) large-area (~ 900 cm^20 module research.

Small-area (0.25 cm^2) Research.

The large-area coated substrate is cut into 2″ x 2″ pieces, and ITO dots are deposited onto the substrate using an evaporation mask. Finally, silver grid lines are deposited by evaporation through a mask. The device area in this case is ~ 0.25 cm^2.

The purpose of the small-area research is to separate the effects of the subsequent module fabrication steps from the basic material quality, thereby making the comparison of the 2B cells with the cells from the small-area deposition system (LINE) possible. Also, the smaller size of devices and substrates is desirable for the evaluation of a large number of cells for light-induced degradation.

The J-V characteristics and *Q* curves of a dual-bandgap, double-junction cell are shown in Fig. 5. The cell efficiency is 11.43%. The values of J_{sc}, V_{oc} and FF are 10.15 mA/cm^2, 1.606 V and 0.701, respectively. The contributions to the J_{sc} from the top and bottom cells are 9.86 and 11.26 mA/cm^2, respectively. The results are tabulated in Table 7.

The J-V characteristics and Q curve of a triple-bandgap, triple-junction cell are shown in Fig. 6. The cell efficiency is 11.15%. The deposition parameters for the triple structure have not been completely optimized. Proper optimization is expected to yield a value of efficiency greater than that obtained in the double-junction case. The values of J_{sc}, V_{oc} and FF are 6.90 mA/cm^2, 2.317 V and 0.697, respectively. The J_{sc} contributions from the top, middle and bottom cells are 6.51, 7.06 and 7.92 mA/cm^2. The results are tabulated in Table 7.

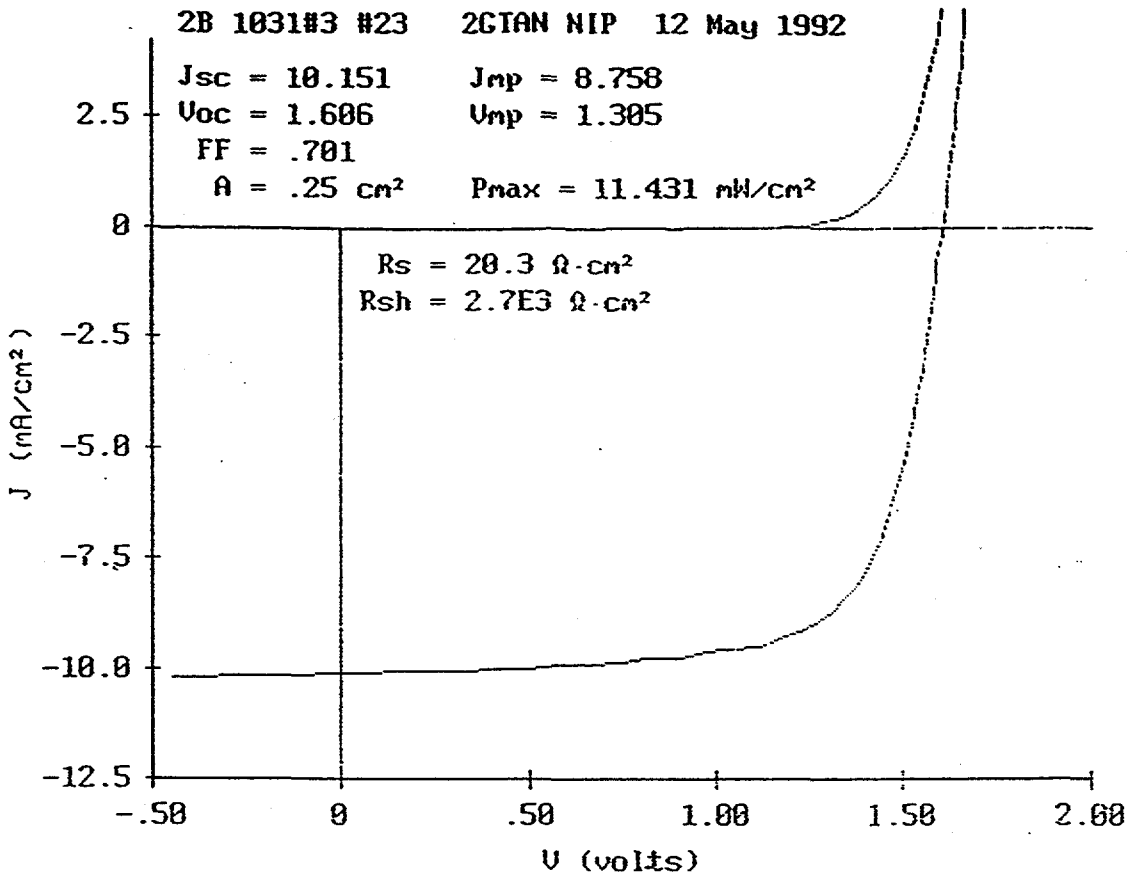

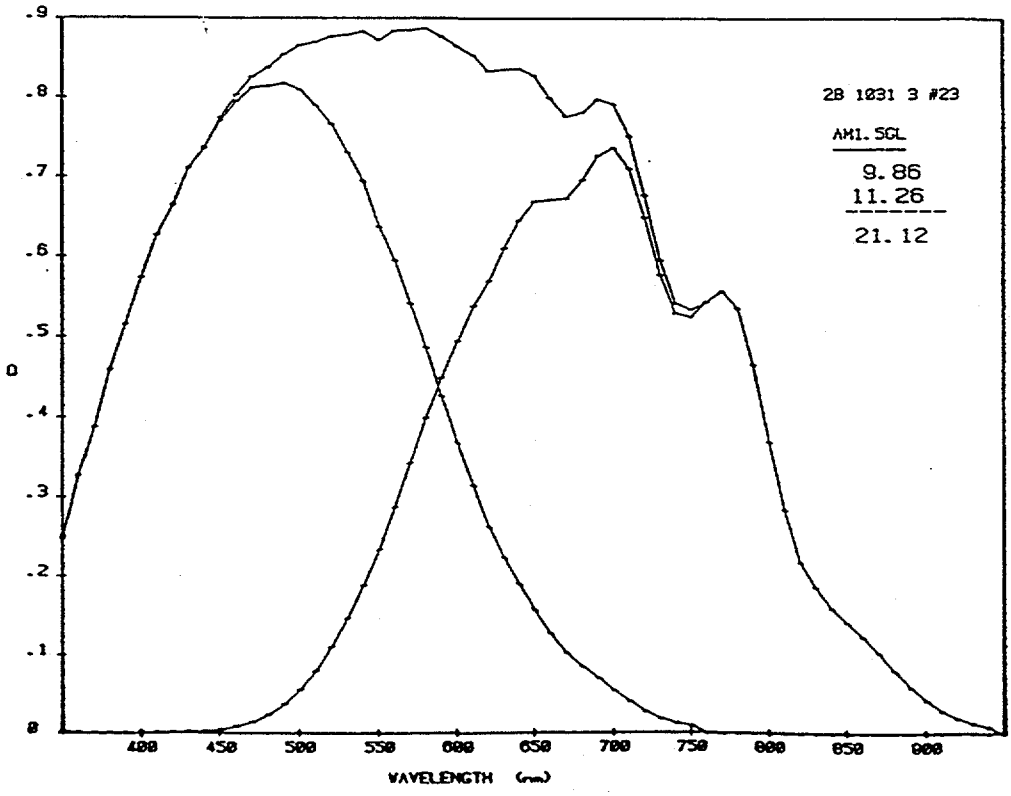

Fig. 5. **J-V characteristics and Q-curve for double-junction cell**

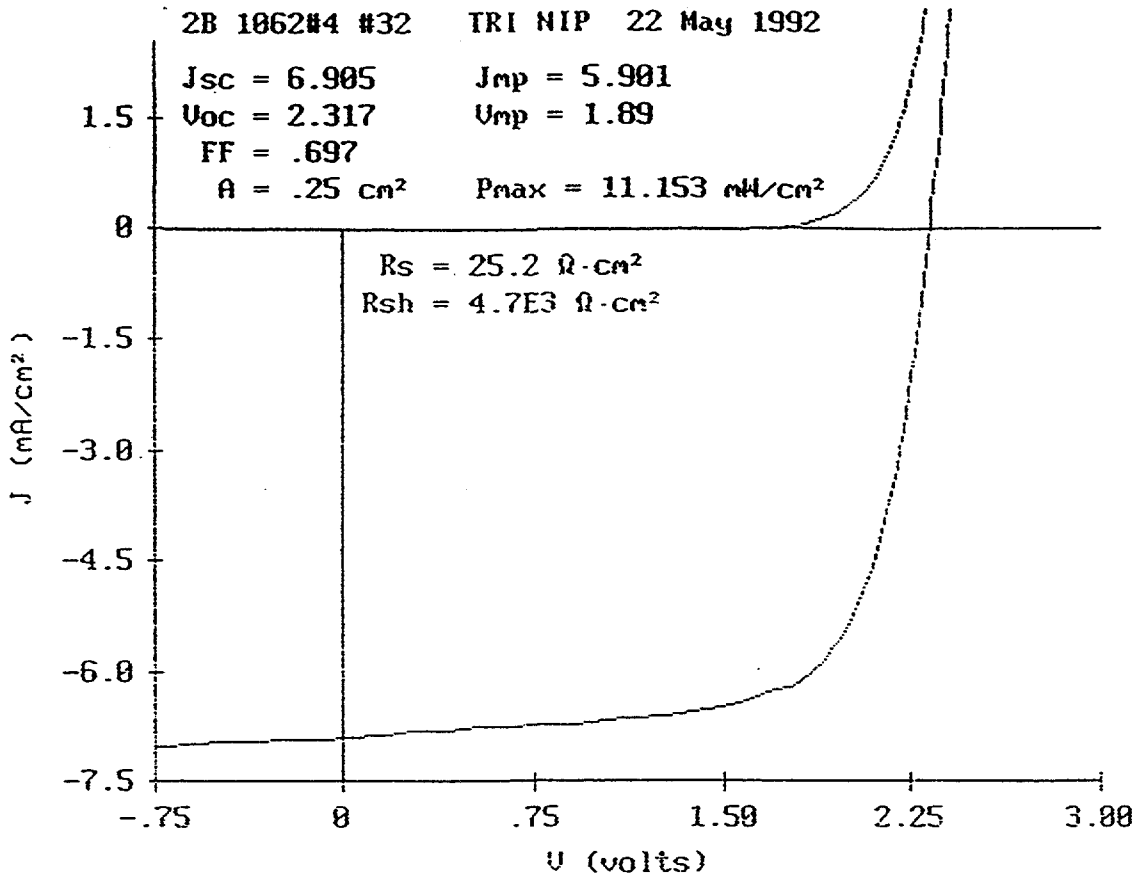

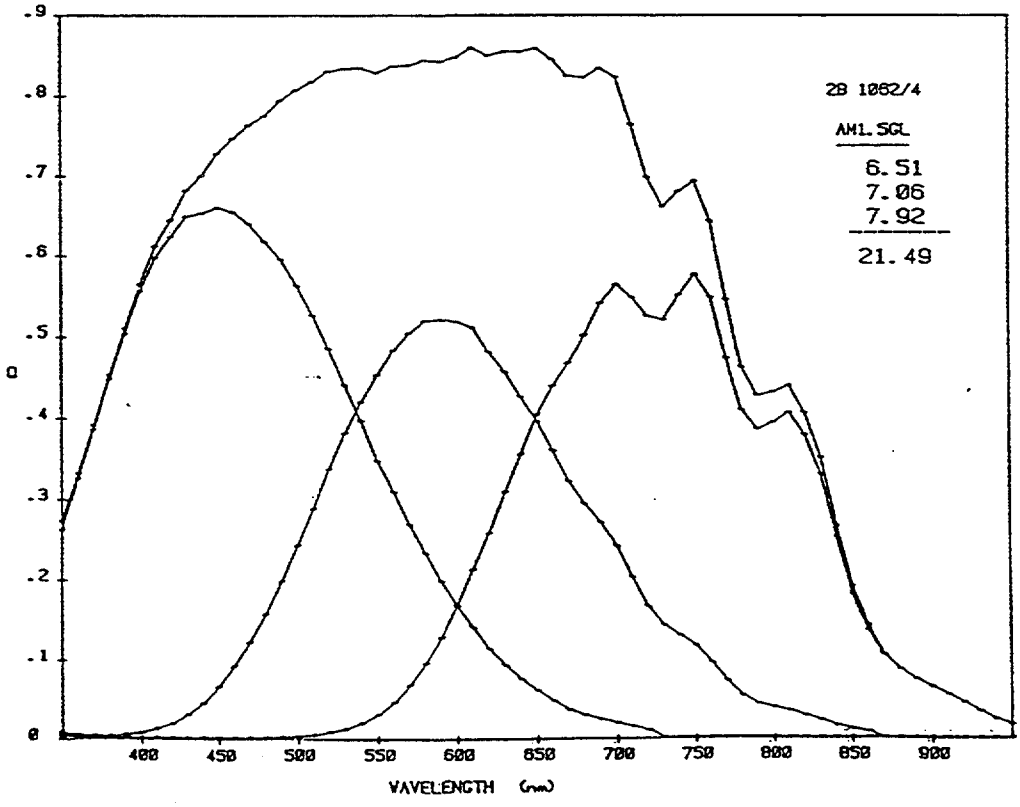

Fig. 6. J-V Characteristics and *Q*-curve for triple-junction cell

Table 7. Summary of I-V Characteristics of Small-area (0.25 cm^2) Cells

Cell Structure	Run #	V_{oc} (V)	J_{sc} (mA/cm2)	FF	η
Dual-Gap double-junction	2B 1031	1.606	10.15 Q_T = 9.86 Q_B = 11.26	0.701	11.43
Triple-Gap triple-junction	2B 1062	2.317	6.90 Q_T = 6.51 Q_M = 7.06 Q_B = 7.92	0.697	11.15

Light-induced degradation studies have been carried out on both the double-junction and triple-junction cells. The results are tabulated in Table 8. All samples have been exposed for about 600 hours to one-sun illumination at 50°C under open-circuit condition. The values of efficiency shown in the table are the average of several devices. The number of exposure hours is shown for each sample. The initial cell efficiency for the double-junction case is ~ 10.5% - 11.1%, and the stabilized efficiency is ~ 8.9% -9.1%. The best value of stabilized efficiency obtained for any device is ~ 9.4%. The initial cell efficiency for the triple-junction case is ~ 10.8%, and the stabilized efficiency is ~ 8.9%.

Table 8. Stability Results

One-sun exposure at 50°C open-circuit condition. Each sample consists of several 0.25 cm^2 active-area devices.

Cell Structure	Sample #	Exposure (hours)	η (Initial)	η (Final)
Dual-gap double-junction	2B 803	593	10.62	9.08
Dual-gap double-junction	2B 880	595	10.51	8.91
Dual-gap double-junction	2B 1031	636	11.10	9.12
Triple-gap triple-junction	2B 1062	640	10.79	8.86

Best stabilized efficiency (double-junction cell) ~ 9.4%

Comparison of the performance of cells made in the large-area 2B machine and those made in the small-area LINE machine shows that the former is worse. We believe that the discrepancy is predominantly due to the poorer material quality of the *i*-layer (both a-Si:H and a-SiGe:H alloys) made in the 2B machine. The possible reasons for the difference are being investigated presently. Also, efforts are under way to further improve the uniformity of deposition in the 2B. Some experiments have already been carried out to address the issues of material quality and deposition uniformity of the *i*-layer and are listed as follows:

1. Vary the deposition temperature.

2. Vary the deposition pressure.

3. Apply dc bias (both positive and negative) to the cathode.

4. Vary the deposition rate.

These experiments have led to some improvements in both material quality and deposition uniformity. The results presented in this report incorporate the improvements. However, further improvements need to be made and currently are being investigated.

Large-area (~ 900 cm^2) Research

The double-junction or triple-junction devices deposited in the 2B machine are coated with ITO over the entire area (> 900 cm^2). The ITO is etched appropriately to delineate the aperture area of the module. The top contact consists of screen-printed silver grid. The coated substrates are next processed for module fabrication, and the results are described in the next section.

Section 4

Module Results

Summary of Module Performance

We have fabricated many dual-gap, double-junction and triple-junction modules of ~ 900 cm^2 area. Figure 7 shows the current voltage characteristics of one of these modules. This module measured 9.6% on a new Spire 240A solar simulator (Including new peak detector circuit board). This module was an all-parallel-area device with an open-circuit voltage of 1.65 volts, short-circuit current of 8.04 A, or 8.91 mA/cm^2 and a fill factor of 64.7%. Table 9 shows a list of several modules measured by NREL and USSC. It is interesting to note that the efficiencies are in excellent agreement between the two labs. However, the measurements of fill factor and short-circuit current are significantly different. We believe the primary difference here is the peak-detector-circuit board which is not installed in the NREL Spire 240A solar simulator.

Table 9. A Summary of Module Results Measured at USSC and NREL

Module #	Location	I_{sc} (A)	J_{sc} (mA/cm^2)	FF	V_{oc} (V)	P_{max} (W)	Area (cm^2)	Eff (%)
1077	USSC	1.27	8.4	0.67	9.97	8.4	909	9.3
	NREL	1.36	9.0	0.60	9.94	8.3	912	9.1
1078	USSC	7.9	8.6	0.65	1.67	8.5	923	9.2
	NREL	8.4	9.1	0.60	1.66	8.3	924	9.0
1103	USSC	7.9	8.8	0.64	1.66	8.4	901	9.3
	NREL	8.3	9.2	0.59	1.67	8.3	903	9.1
1118	USSC	8.0	8.9	0.65	1.65	8.6	902	9.6
	NREL	8.6	9.5	0.59	1.65	8.4	903	9.3

Table 10 shows a comparison of efficiency measurements made at NREL and USSC on two dual-junction modules of ~ 900 cm^2 area. This table shows the I-V parameters, type of test, module measured and the temperature-corrected efficiencies based on temperature coefficient measurements. The outdoor temperature measurements were made at the back of the module, which has considerable thermal insulation from the device itself. Therefore, we have added a temperature correction based on the open-circuit voltage differences measured indoors and outdoors using the power temperature coefficient shown in Fig. 9. These temperatures and temperature-corrected parameters are shown below the outdoor-measured parameters in parenthesis. We can see from this data that the USSC results agree with the NREL outdoor measurements within about 4%.

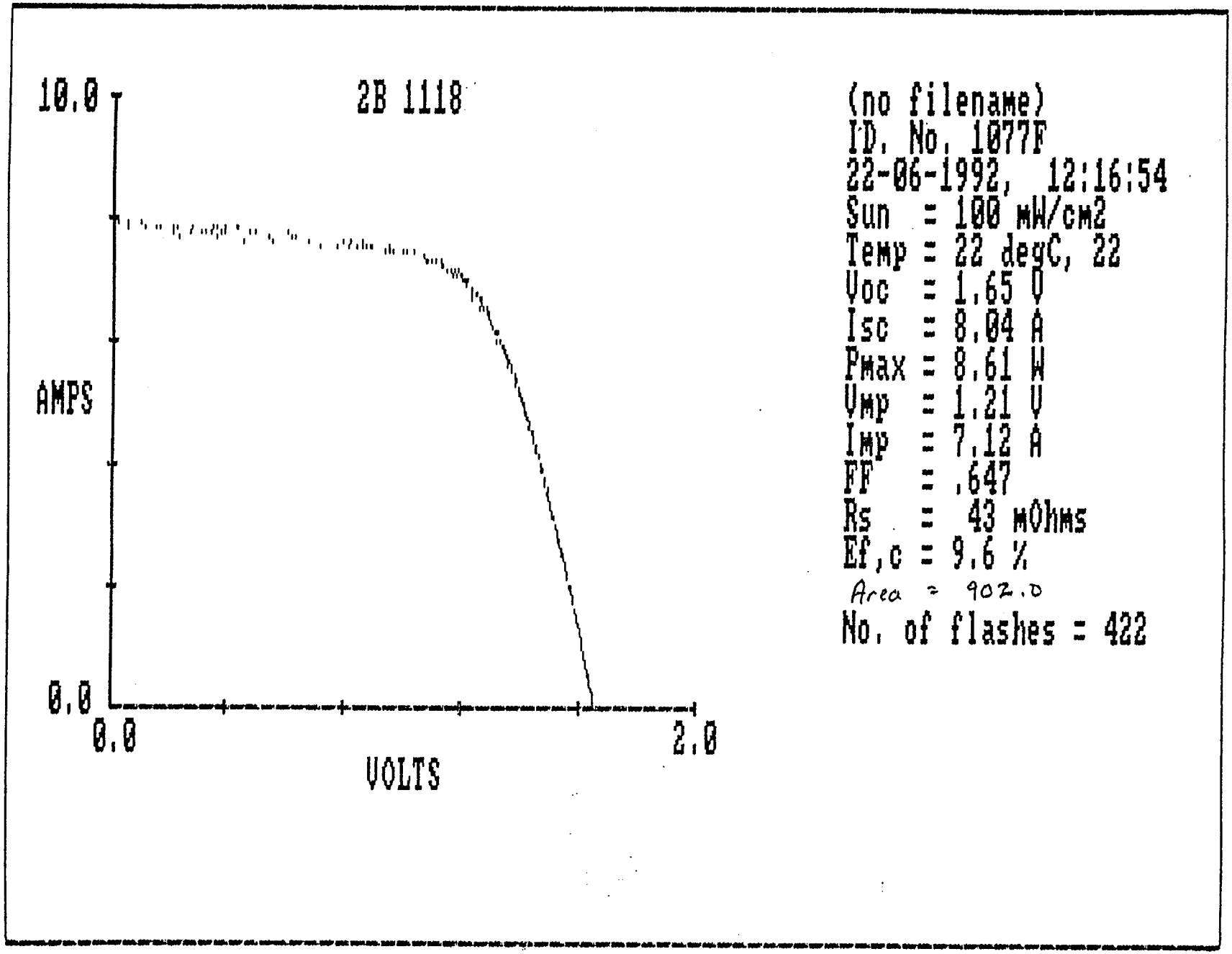

Fig. 7. I-V characteristics of a monolithic double-junction module

Table 10. A Comparison of Dual-junction Module Measurements at USSC and NREL

Module	Type of Test	T (TV) (C)	I_{sc} (A)	V_{oc} (V)	FF	Eff (%)
2B 935	NREL Spire	25	1.31	0.985	0.611	8.53
	NREL Outdoor	34	1.27	0.937	0.654	8.41
	(Temp. Corrected)	(43)	(1.25)	(0.985)	(0.643)	(8.59)
	USSC Spire	25	1.27	9.87	0.655	8.91
2B 936	NREL Spire	25	1.32	9.84	0.603	8.50
	NREL Outdoor	31	1.28	9.58	0.638	8.48
	(Temp. corrected)	(35)	(1.26)	(9.84)	(0.632)	(8.54)
	USSC Spire	25	1.28	9.83	0.649	8.90

(TV) = Temperature corrected to Voltage at 25°C

In addition to these module measurements, we have fabricated six single-junction modules of different bandgap and area to evaluate the electrical measurements of the Spire 240A solar simulator. We chose to use single-junction devices so as to minimize any dependence of device fill factor on spectral content of the illuminating spectrum. We compared fill factor measurements for these modules measured with the Spire 240A simulator and a DC Oriel solar simulator to compare the DC measurement under the Oriel with the transient-type measurement of the Spire. Table 11 shows that in no case did the difference in the two types of measurement exceed 2%. This indicates that capacitance effects do not influence the measurements under Spire 240A simulator which has a pulsed illumination. The samples have been sent to NREL for evaluation of their simulator.

Table 11. A Comparison of Fill Factor Measurements for a DC Solar Simulator and a Pulsed Spire 240A Solar Simulator

Type	Area (cm^2)	Spire 240A	Oriel (DC)
a-SiGe	200	0.594	0.584
a-SiGe	100	0.620	0.608
a-SiGe	100	0.579	0.579
a-Si	200	0.557	0.566
a-Si	100	0.568	0.579
a-Si	100	0.566	0.576

Reliability Test of Modules

We have begun reliability testing on small modules (150 cm^2). The results of the first test, 20 thermal cycles from -40°C to +90°C, are shown in Table 12. These small modules were a-Si/a-SiGe double-junction cells on Ag/ZnO back reflectors on stainless steel substrates. These devices were fabricated in the same manner as the one-square-foot modules. This table shows the results of efficiency measurements performed before and after thermal cycling.

Table 12. Effect of Thermal Cycling on Module Efficiency

	Condition: -40°C to +90°C, Dark	
	Efficiency (% Change)	
Sample #	0 (cycles)	50 (cycles)
2B 928 C	8.5	8.2 (-4%)
2B 933 F	8.5	8.4 (-1%)
2B 937 D	8.4	8.3 (-1%)

From Table 12, we observe very little change in the electrical performance of the small modules due to the thermal cycling.

Module Instability

We have continuously light-soaked two multijunction modules, one double-junction and one triple-junction, at one sun for approximately 700 hours. The triple-junction module degraded from an initial efficiency of 9.6% to a final saturated efficiency of 8.1% as measured by the Spire 240 at USSC. For the double-junction module, we observed an initial efficiency of 9.4% and final saturated efficiency of 8.1%. Figure 8 shows a graph of the efficiency versus time for both modules. Note that repeatability of the measurements is typically ± 2%. Both modules were degraded under at one sun under metal halide lamps and reached a temperature of 57°C. Table 13 shows the initial and final I-V parameters for both modules.

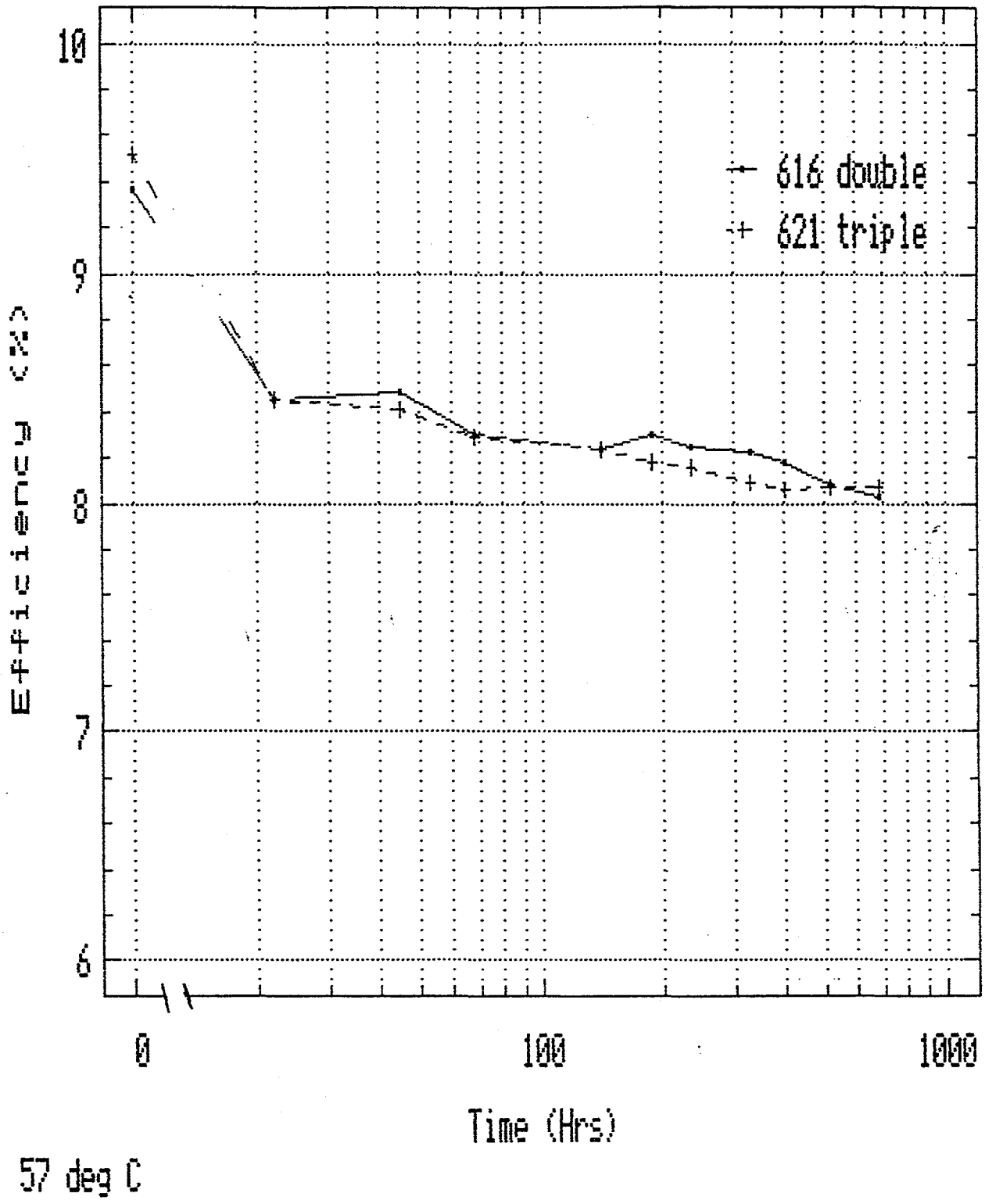

Fig. 8. **Stability of double- and triple-junction modules**

Table 13. Instability of Double- and Triple-junction Modules as a Result of Light-soaking for 700 Hours at One Sun

Module #	I-V Parameter	Initial	Final	Change
616 (double)	Efficiency (%)	9.4	8.1	-14%
	J_{sc} (mA/cm^2)	8.9	8.8	- 1%
	V_{oc} (Volts)	1.60	1.50	- 6%
	FF (%)	66	61	- 7%
621 (triple)	Efficiency (%)	9.6	8.1	-16%
	J_{sc} (mA/cm^2)	6.0	5.9	- 2%
	V_{oc} (Volts)	2.40	2.30	- 4%
	FF (%)	67	60	-10%

Temperature Coefficients

We have measured the temperature coefficients for short-circuit current, open-circuit voltage, fill factor and power for a dual-gap, double-junction device. Figure 9 shows the results in graphic form. This device was a small-area cell (0.25 cm^2) fabricated by the same deposition machine and parameters as the modules described earlier. It is important to note that the power coefficient is negative throughout the range of temperatures that would normally be seen in an outdoor measurement. This difference is significant and is in the range of a 2% - 3% correction factor for outdoor performance evaluation.

Future Directions

Although significant progress has been made in our program in the last six months with the initial module aperture-area efficiency increasing from 7.8% to 9.3% as measured at NREL, further improvements are necessary to reach the 10% stable efficiency goal by the end of this year. The major thrust should be to reduce the gap between the efficiencies obtained in the small-area (LINE) and the large-area (2B) deposition reactors. We have demonstrated 11% stabilized active-area efficiency in the small-area reactor, which should be translated into 10% stabilized aperture-area efficiency. The 2B machine is more than ten years old, and we are now making a major modification of the deposition area of the chamber so that all the components used are of high quality. We are also improving the deposition uniformity so that the gap between the best and the average subcell efficiency over one-square-foot area is lowered below the current 5%. Finally, even though the grid losses are significantly reduced, further efforts are in progress to improve the shadow losses. Once all these improvements are in place, 10% stable module efficiency should be achieved.

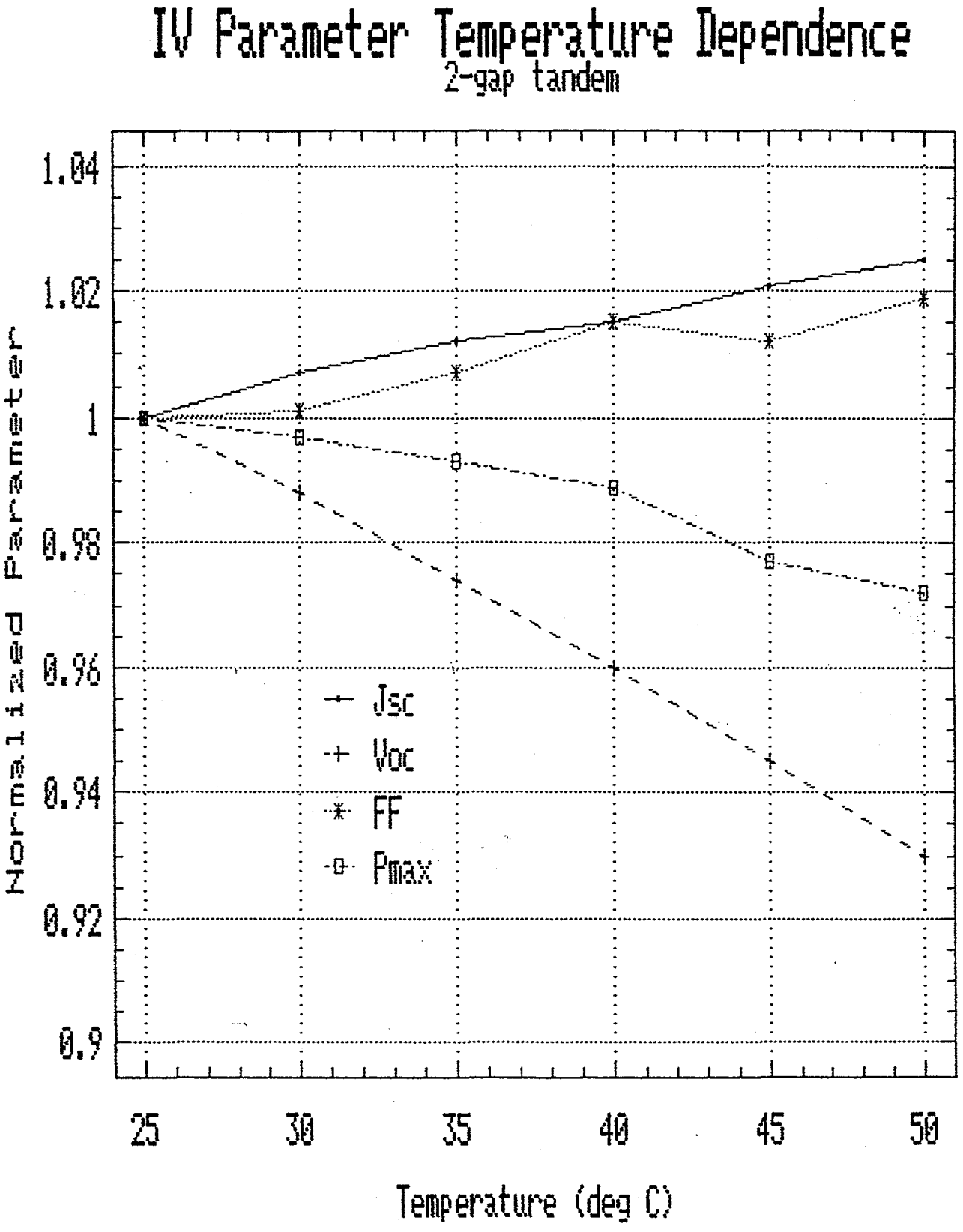

Fig. 9. **Temperature dependence of electrical parameters of double-junction cell**

References

1. For recent publications on this subject, see *Amorphous Silicon Materials and Solar Cells*, edited by B. L. Stafford (American Institute of Physics Conf. Proc. 234, New York, 1991).

2. S. Guha, J. Yang, W. Czubatyj, S. J. Hudgens and M. Hack, Appl. Phys. Lett. 42, 588 (1983).

3. C. R. Wronski and N. Maley, in *Amorphous Silicon Materials and Solar Cells*, edited by B. L. Stafford (American Institute of Physics Conf. Proc. 234, New York, 1991), p. 11.

4. D. L. Williamson, A. H. Mahan, B. P. Nelson and R. S. Crandall, J. Non-cryst. Solids, 114, 226 (1989).

5. A. H. Mahan, D. L. Williamson, B. P. Nelson and R. S. Crandall, Phys. Rev. B 40, 12024 (1989).

6. A. H. Mahan, D. L. Williamson, B. P. Nelson and R. S. Crandall, Solar Cells, 27, 465 (1989).

7. S. Guha, Final Report, SERI/TP-211-3918 (Solar Energy Research Institute, Golden, Colorado, 1990).

8. D. L. Williamson, A. H. Mahan, B. P. Nelson and R. S. Crandall, Appl. Phys. Lett. 55, 783 (1989).

9. A. Guinier, *X-ray Diffraction in Crystals, Imperfect Crystals and Amorphous Bodies* (W. H. Freeman, San Francisco, 1963), p. 264.

10. E. Bhattacharya and A. H. Mahan, Appl. Phys. Lett. 52, 1587 (1988).

11. A. Langford, M. Fleet, B. P. Nelson, W. A. Lanford and N. Maley, Phys. Rev. B45, 13367 (1992).

12. A. Matsuda, S. Mashima, K. Hasezaki, A. Suzuki, S. Yamasaki and P. J. McElheny, Appl. Phys. Lett. 58, 2494 (1991).

13. W. Den Boer and S. Guha, J. Appl. Phys. 57, 5539 (1985)

14. M. Stutzmann, W. B. Jackson and C. C. Tsai, Phys. Rev. B 34, 63 (1986).

15. S. Guha, C. Y. Huang and S. J. Hudgens, Appl. Phys. Lett. 45, 50 (1984).

16. R. S. Crandall, Phys. Rev. B 43, 4057 (1991).

17. W. B. Jackson and N. M. Amer, Phys. Rev. B 25, 5559 (1982); M. Vanecek, J. Kocka, J. Stuchlik, Z. Kozisek, O. Stika and A. Triska, Sol. Energy Mat., 8, 411 (1983).

18. X. R. Li, S. Wagner and M. Bennett, Mat. Res. Soc. Symp. Proc. Vol. 258 (to be published).

19. See, for example, N. W. Wang, X. Xu and S. Wagner, in Ref. 1, p. 186.

20. S. Guha, J. S. Payson, S. C. Agarwal and S. R. Ovshinsky, J. Non-cryst. Solids, 97 & 98, 1455 1988).

21. S. Guha, J. Yang, S. J. Jones, Y. Chen and D. L. Williamson (to be published).

22. Q. Wang, H. Antoniadis, E. A. Schiff and S. Guha, Mat. Res. Soc. Symp. Proc. Vol. 258 (to be published).

23. J. Yang, R. Ross, T. Glatfelter, R. Mohr, and S. Guha, Mat. Res. Soc. Symp. Proc. Vol. 149, P. 435 (1989).

24. S. Guha, J. Yang, A. Pawlikiewicz, T. Glatfelter, R. Ross, and S. R. Ovshinsky, Appl. Phys. Lett. 54, 2330 (1989).

Document Control Page	1. NREL Report No. NREL/TP-411-5063	2. NTIS Accession No. DE93000011	3. Recipient's Accession No.

4. Title and Subtitle

Research on Stable, High-Efficiency Amorphous Silicon Multijunction Modules

5. Publication Date

September 1992

6.

7. Author(s)

S. Guha

8. Performing Organization Rept. No.

9. Performing Organization Name and Address

United Solar Systems Corporation
Troy, Michigan

10. Project/Task/Work Unit No.
PV241101

11. Contract (C) or Grant (G) No.

(C) ZM-1-19033-2

(G)

12. Sponsoring Organization Name and Address
National Renewable Energy Laboratory
1617 Cole Blvd.
Golden, CO 80401-3393

13. Type of Report & Period Covered
Technical Report
1 January 1992 - 30 June 1992

14.

15. Supplementary Notes
NREL technical monitor: W. Luft

16. Abstract (Limit: 200 words)

This report describes research on semiconductor and non-semiconductor materials to enhance the performance of multi-band-gap, multijunction, large-area, amorphous-silicon-based alloy modules. The goal is to demonstrate a stabilized module efficiency of 10% for a multijunction panel with an area greater than 900 cm^2 by 1992. Double-junction and triple-junction cells are made on a Ag/ZnO back reflector deposited on stainless steel substrates. An a-SiGe alloy is used for the i-layer in the bottom and the middle cells; the top cell uses an amorphous silicon alloy. After the evaporation of an antireflection coating, silver grids and bus bars are put on the top surface and the panel is encapsulated in an ethylene vinyl acetate (EVA)/Tefzel structure to make a 1-ft^2 monolithic module.

17. Document Analysis
a. Descriptors
high efficiency ; amrophous silicon ; modules ; photovoltaics ; solar cells

b. Identifiers/Open-Ended Terms

c. UC Categories
271

18. Availability Statement
National Technical Information Service
U.S. Department of Commerce
5285 Port Royal Road
Springfield, VA 22161

19. No. of Pages
38

20. Price
A03

Form No. 0069E (6-30-87)